Solvation and Hydrogen-Bonding Effects on Proton Wires

ARTICLE *in* THE JOURNAL OF PHYSICAL CHEMISTRY A · MARCH 1999

Impact Factor: 2.69 · DOI: 10.1021/jp984775u

3 AUTHORS, INCLUDING:

Karen Drukker
University of Chicago
87 PUBLICATIONS **1,064** CITATIONS

SEE PROFILE

Solvation and Hydrogen-Bonding Effects on Proton Wires

Hélène Decornez, Karen Drukker, and Sharon Hammes-Schiffer*

Department of Chemistry and Biochemistry, University of Notre Dame, Notre Dame, Indiana 46556

Received: December 17, 1998; In Final Form: February 17, 1999

In this paper, the multiconfigurational molecular dynamics with quantum transitions (MC-MDQT) method is used to simulate the nonequilibrium real-time quantum dynamics of proton transport along water chains in the presence of solvating water molecules. The model system consists of a protonated chain of three water molecules and two additional solvating water molecules hydrogen-bonded to each end of the chain. Nonequilibrium initial configurations are generated with an extra proton stabilized on one end of the water chain, and proton transport along the chain is induced by variations in the hydrogen-bonding distances between the solvating water molecules and the ends of the chain. These simulations indicate that solvation and hydrogen bonding significantly impact the proton-transport process and that quantum effects such as hydrogen tunneling and nonadiabatic transitions play an important role. Moreover, this model system exhibits a wide range of mechanisms, including both concerted and sequential double proton transfer, both strongly and weakly coupled double proton transfer, and both adiabatic and nonadiabatic pathways. The MC-MDQT approach provides a clear physical framework for interpreting and analyzing these different types of mechanisms.

I. Introduction

Hydrogen-bonded chains of water molecules have been observed experimentally in a number of proteins, including photosynthetic reaction centers[1] and cytochrome *f*.[2] These water chains are thought to play an important role in the translocation of protons over large distances in proteins. The postulated mechanism for these "proton wires" is that a proton is deposited on one end of the water chain and is transported to the other end of the chain through a series of proton-transfer steps.[3]

Proton transport in water has been simulated with a wide range of methodology.[4−20] In terms of proton wires, Pomès and Roux have used Feynman path integral quantum dynamical methods to study the equilibrium properties of isolated protonated water chains[4,5] and more recently have used classical molecular dynamics methods to generate free energy profiles for protonated water chains in the presence of solvent droplets.[6] While these simulations have provided great insight into the proton transport process, this methodology does not provide real-time dynamical information.

The multiconfigurational molecular dynamics with quantum transitions (MC-MDQT) method was developed for the nonequilibrium real-time quantum dynamical simulation of multiple proton transfer reactions.[21,22] Recently, MC-MDQT was used to study proton transport along protonated chains of three and four water molecules.[23] In these simulations, nonequilibrium starting configurations were generated by applying an external electric field that stabilized the extra proton on one end of the chain, and the proton transport process was induced by increasing the electric field linearly in time until the extra proton was stabilized on the other end of the chain. These conditions were designed to mimic the mechanism described above for proton wires in proteins. In these simulations, the ramping speed of the electric field completely determined the rate of proton transfer, and under these rigidly controlled conditions, the proton transfer reactions were always sequential and only weakly coupled.

In this paper, we apply MC-MDQT to a model system consisting of a protonated chain of three water molecules and two additional solvating water molecules hydrogen-bonded to each end of the chain. Instead of applying an external electric field, we apply restraints on the solvating water molecules to generate nonequilibrium starting configurations in which the extra proton is stabilized on one end of the chain. Specifically, we restrain the solvating water molecules on one end of the chain to relatively short hydrogen-bonding distances with the chain. The proton transport process is induced by releasing these restraints. (As discussed in ref 17, hydrogen-bonding distances greatly impact the stabilization of H_3O^+.) This approach is motivated by the situation in a protein environment in which the water chain forms hydrogen bonds to the protein[24] or, in some cases, the ends of the water chain are in contact with the external solvent.[25] In contrast to our simulations with strong external electric fields, we observe a wide range of dynamical mechanisms, including both concerted and sequential double proton transfer, both strongly and weakly coupled double proton transfer, and both adiabatic and nonadiabatic pathways. This application illustrates the power of the MC-MDQT approach in providing a clear physical framework for interpreting and analyzing different types of dynamical mechanisms.

An outline of this paper is as follows. Section II describes the MC-MDQT methodology, the model system, the simulation details, and the procedure used to generate the nonequilibrium starting configurations. Section III presents statistical results obtained from a large number of trajectories and detailed analyses of five different types of trajectories. Conclusions are discussed in section IV.

II. Methods

A. MC-MDQT. A number of mixed quantum/classical molecular dynamics methods have been applied to proton transfer reactions in solution.[26−48] Typically, the transferring hydrogen atom(s) are treated quantum mechanically, while the remaining nuclei are treated classically. In this paper, we utilize

10.1021/jp984775u CCC: $18.00
Published on Web 03/30/1999

the MC-MDQT method,[21,22] which combines an MC-SCF calculation of the vibrational wave function with the MDQT surface hopping method. In this section we present only a brief outline of MC-MDQT since it is discussed in detail elsewhere.[49,50]

The fundamental principle of MDQT is that an ensemble of trajectories is propagated, and each trajectory moves classically on a single adiabatic surface except for instantaneous transitions among the adiabatic states. The instantaneous adiabatic states $\Phi_n(\mathbf{r};\mathbf{R})$ are calculated at each classical molecular dynamics time step by solving the time-independent Schrödinger equation

$$H_q(\mathbf{r},\mathbf{R})\Phi_n(\mathbf{r};\mathbf{R}) = \epsilon_n(\mathbf{R})\Phi_n(\mathbf{r};\mathbf{R}) \tag{1}$$

where $\mathbf{r}$ and $\mathbf{R}$ indicate the quantum and classical coordinates, respectively, and H_q is the sum of the kinetic energy of the quantum coordinates and the total potential energy. The classical nuclei evolve according to standard classical equations of motion with the effective potential

$$V_{\text{eff}} = \langle \Phi_k | H_q | \Phi_k \rangle \tag{2}$$

where Φ_k is the occupied adiabatic state. The time-dependent wave function describing the quantum subsystem is expanded in a basis of the instantaneous adiabatic states:

$$\Psi(\mathbf{r},\mathbf{R},t) = \sum_n C_n(t)\Phi_n(\mathbf{r};\mathbf{R}) \tag{3}$$

and the quantum amplitudes $C_n(t)$ are calculated by integrating the time-dependent Schrödinger equation simultaneously with the classical equations of motion. At each time step, Tully's "fewest switches" algorithm[41,51] is invoked to determine if a quantum transition to another adiabatic state should occur. This algorithm correctly apportions trajectories among the adiabatic states according to the quantum probabilities $|C_n(t)|^2$ with the minimum required number of quantum transitions (neglecting difficulties with classically forbidden transitions).[52]

The simulation of multiple proton transfer reactions requires the quantum mechanical treatment of multiple hydrogen atoms, which leads to multidimensional proton vibrational wave functions $\Phi_n(\mathbf{r};\mathbf{R})$. We designed an MC-SCF formulation to calculate these proton vibrational wave functions (i.e., to solve eq 1).[21,22] This method incorporates the significant correlation among the quantum protons in a computationally efficient manner. In this formulation, the adiabatic states for a system of N quantum protons are approximated by a normalized linear combination of single configurations:

$$\Phi_n(\mathbf{r};\mathbf{R}) = \sum_J^Q d_{nJ}\xi_J(\mathbf{r};\mathbf{R}) \tag{4}$$

where the single configurational wave functions $\xi_J(\mathbf{r};\ \mathbf{R})$ are products of the orthonormal one-particle states $\phi_{j_k}^{(k)}$:

$$\xi_J(\mathbf{r};\mathbf{R}) = \prod_{k=1}^N \phi_{j_k}^{(k)}(r_k;\mathbf{R}) \tag{5}$$

Here $J = (j_1, j_2, ..., j_N)$ and Q is the total number of configurations. Each one-particle state $\phi_j^{(k)}(r_k;\mathbf{R})$ can be expanded in an appropriate fundamental basis set. In this paper, each quantum proton moves in only one dimension and the fundamental basis functions are chosen to be real. Application of the variational principle to the total energy leads to a set of matrix equations that must be solved self-consistently to obtain the one-particle states and the configuration interaction coefficients d_{nJ}.

At each MDQT time step, a physically reasonable initial wave function is chosen by invoking the effective one-particle Hamiltonians proposed in ref 21. In this approach, the one-particle wave functions are calculated by solving the set of N eigenvalue equations

$$h_{\text{eff}}^{(k)}\phi_j^{(k)}(r_k) = \epsilon_j^{(k)}\phi_j^{(k)}(r_k) \tag{6}$$

where

$$h_{\text{eff}}^{(k)} = t_k + \sum_J^Q d_{nJ}^2 \left\langle \prod_{i\neq k}^N \phi_{j_i}^{(i)}(r_i) \middle| V(\mathbf{r},\mathbf{R}) \middle| \prod_{i\neq k}^N \phi_{j_i}^{(i)}(r_i) \right\rangle \tag{7}$$

Here, t_k is the kinetic energy of quantum mode k, $V(\mathbf{r},\mathbf{R})$ is the total potential energy of the system, and n indicates the occupied multiconfigurational adiabatic state. Note that, for single configurational wave functions ($Q = 1$), the self-consistent solution of eqs 6 and 7 produces a variational wave function.

The MC-MDQT methodology can be summarized as follows. At each classical time step the MC-SCF formulation is utilized to obtain the instantaneous adiabatic proton vibrational states. The classical nuclei evolve according to an effective potential derived from the occupied multiconfigurational adiabatic state. The time-dependent Schrödinger equation is integrated simultaneously with the classical equations of motion to obtain the quantum probabilities for the adiabatic states. Instantaneous transitions are incorporated among the adiabatic states in a way that ensures that, for an ensemble of trajectories, the fraction in any state at any time is the quantum probability for that state.

The MC-MDQT method has been tested thoroughly. References 54 and 55 illustrate that the MDQT method accurately reproduces fully quantum dynamical calculations for one-dimensional model systems representing both single and double proton transfer. Moreover, ref 22 shows that the MC-SCF method accurately reproduces the forces and the four lowest energy states obtained from full configuration interaction calculations for a protonated chain of three water molecules. Thus, we expect that the main source of error in our simulations is the model used to represent the water chains rather than the MC-MDQT methodology.

B. Simulation Procedure. In this paper, we use the PM6 dissociable and polarizable water model developed by Stillinger and co-workers.[56−58] This model is appropriate for the study of proton transport since it allows bonds to break and form. Moreover, this model gives a qualitatively (but not quantitatively) accurate picture of proton transfer, with increasing barrier heights corresponding to increasing distances between the donor and acceptor oxygen atoms. We are in the process of implementing a more accurate multistate empirical valence bond potential for water recently developed by Schmitt and Voth.[8]

In our simulations, only the two protons that form hydrogen bonds within the water chain are treated quantum mechanically. All oxygen atoms and the remaining hydrogen atoms are treated classically. The classical protons are constrained to a fixed O−H bond length in order to avoid nonphysical vibrational coupling between the quantum and classical protons. The angle within each water molecule is not constrained, however, and the water molecules are allowed to bend and rotate freely. Note that reorientations of the water molecules are not allowed, but such reorientations are not expected to occur on the fast time scale of the proton transport process studied in this paper. The

classical equations of motion are integrated using the RATTLE method for constrained molecular dynamics,[59] which is based on the velocity Verlet algorithm, using a time step of $\Delta t = 0.0625$ fs. The quantum protons are restricted to move in one dimension along the oxygen−oxygen axes; i.e., the quantum proton wave functions are represented on one-dimensional grids along the O−O axes. These grids span 3 Å and are centered around the midpoint of the relevant oxygen−oxygen axis for each quantum proton. We use 51 grid points per one-dimensional grid, and for each quantum proton we use 18 one-particle basis functions consisting of 3 sets of 6 basis functions centered roughly around the positions of the potential minima for a double well potential and a single well potential, respectively. The basis functions are chosen as Hermite polynomials (represented on a grid) with the characteristic frequency of $\omega = 2000$ cm^{-1}. We include nine configurations in our expansion of the MC-SCF adiabatic wave functions, and the MC-MDQT calculations include the three adiabatic states lowest in energy.

The generation of the nonequilibrium initial configurations for our MC-MDQT simulations entails three distinct stages. The first stage involves the classical equilibration of a chain of three water molecules at 300 K using a Nosé heat bath.[60,61] (To keep the chain linear it is placed in a channel as described in ref 22.) After initial equilibration, a configuration is stored every picosecond for input into the second stage. The second stage involves the classical dynamical preparation of protonated water chains with two solvating water molecules at each end of the chain. For each configuration from the first stage, an extra proton is added to one end of the chain. Subsequently, two solvating water molecules are placed at an O−O distance of 2.6 Å at the protonated end of the chain, and two solvating water molecules are placed at an O−O distance of 2.87 Å (which is approximately the average O−O distance in a neutral water chain for this model) at the other end of the chain. This positioning of the solvating water molecules stabilizes the H_3O^+ on one end of the chain. Strong harmonic restraints (with force constants $k = 1000$ kcal/mol Å^{-2}) are placed on all oxygen atoms to maintain this type of configuration. Classical molecular dynamics simulations at 300 K are performed on these systems with a Nosé heat bath. The third stage involves the quantum dynamical relaxation of the configurations generated from the second stage. At this stage, MC-MDQT simulations are performed for 6.25 fs, and all configurations that result in proton transfer or nonadiabatic transitions during this short quantum simulation are discarded. (In our simulations, 107 out of 500 configurations were discarded in this third stage.) The remaining configurations are used for the MC-MDQT simulations described in section III. Figure 1a depicts a sample starting configuration in which the solvating waters on the left are closer to the chain than are the solvating waters on the right. As a result, the "extra" proton is stabilized on the left end of the chain.

These nonequilibrium starting configurations represent the situation in a protein environment where an extra proton is deposited at one end of the chain. The proton transport process is induced by releasing the restraints on the oxygen atoms of the two solvating water molecules that stabilize the extra proton (i.e., on the left end of the chain in Figure 1). The restraints on the oxygen atoms of the other two solvating molecules are kept the same (with a large force constant of $k = 1000$ kcal/mol Å^{-2}) to maintain typical O−O distances with the chain. The restraints on the oxygen atoms of the chain water molecules, however, are decreased (with a force constant of $k = 100$ kcal/mol Å^{-2}) to allow them to fluctuate slightly as in a protein channel environment. The nonequilibrium MC-MDQT simulations are performed without the Nosé heat bath. Snapshots from a real-time MC-MDQT simulation are depicted in Figure 1. Note that at the beginning the left solvating water molecules are closer to the chain, while at the end the right solvating water molecules are closer to the chain.

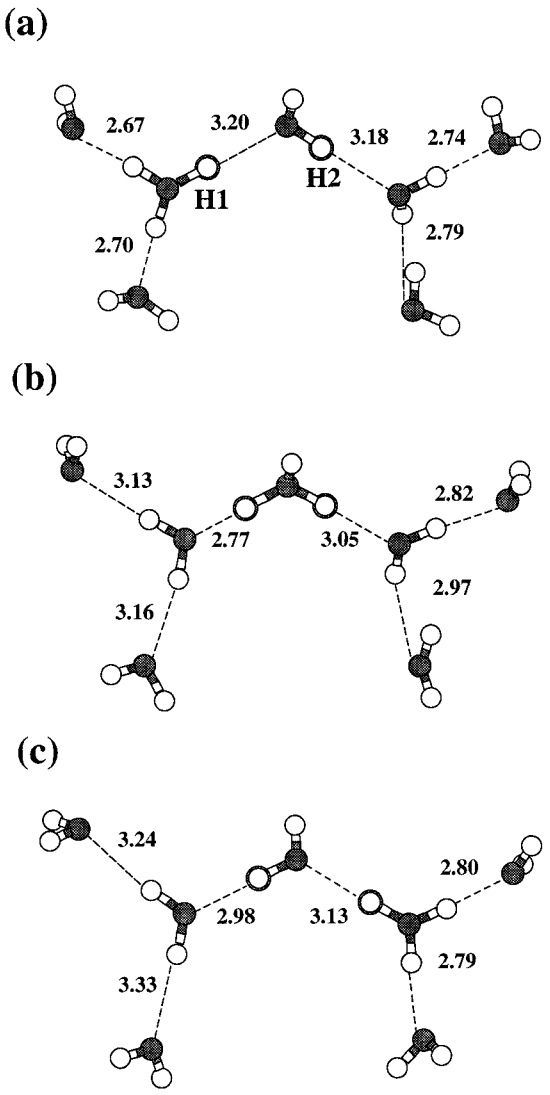

Figure 1. Snapshots of representative configurations during a sample trajectory of a protonated chain of three water molecules with two solvating water molecules at each end of the chain. Dashed lines indicate hydrogen bonds with corresponding oxygen−oxygen distances given. The quantum protons H1 and H2 are placed at the expectation values of their coordinates and are highlighted in each configuration. Snapshots are depicted at (a) $t = 0.000$ fs, (b) $t = 15.688$ fs, and (c) $t = 60.938$ fs.

III. Results

We generated 393 nonequilibrium starting configurations from the procedure described above, and 89 of the resulting MC-MDQT trajectories exhibited double proton transfer in less than 87.5 fs. (Double proton transfer is defined to occur when each proton has formed a bond with its acceptor and the system is in the ground vibrational state. Here an OH bond is defined to be formed when the distance between the oxygen and the expectation value of the proton coordinate is less than 1.175 Å.) Typically, the trajectories that did not exhibit double proton transfer in the allotted time resulted in stable configurations where the extra proton was localized in a single well

TABLE 1: Fraction of 89 Trajectories That Exhibit Each Type of Mechanism

	concerted (strongly coupled)	sequential (strongly coupled)	sequential (weakly coupled)
adiabatic	0.10	0.19	0.57
nonadiabatic	0.00	0.05	0.09

TABLE 2: Distances between Pairs of Oxygen Atoms in the Model System at the Beginning of the Double Proton Transfer Reaction for Strongly and Weakly Coupled Trajectories[a]

O−O pair	strongly coupled	weakly coupled
left solvent−H1 donor	2.81 (.02)	2.83 (.01)
right solvent−H2 acceptor	2.80 (.01)	2.80 (.004)
H1 donor−H1 acceptor	3.05 (.02)	2.95 (.01)
H2 donor−H2 acceptor	2.96 (.02)	2.98 (.02)

[a] The notation for the O−O pairs refers to Figure 1. The left solvent−H1 donor and right solvent−H2 acceptor distances are averaged over the two solvating water molecules on the left and right, respectively. The numbers in parentheses indicate rms deviations. All distances are given in angstroms.

between the middle and right water molecules of the chain. These trajectories were not included in our analysis since the proton-transport process was not complete.

The 89 double proton transfer trajectories exhibited a wide range of different dynamical behavior. We observed both concerted and sequential double proton transfer. Trajectories were labeled *concerted* when the two proton-transfer reactions occurred within 0.5 fs (i.e., when the time between the first proton breaking the bond with its donor and the second proton forming the bond with its acceptor was less than 0.5 fs). All other trajectories were labeled *sequential*. In addition, we observed both strongly and weakly coupled double proton transfer. Trajectories were labeled *strongly coupled* when the second proton was at least half transferred within 0.5 fs of the completion of the first proton transfer (i.e., when the time between the first proton forming the bond with its acceptor and the second proton becoming delocalized over both wells was less than 0.5 fs). All other trajectories were labeled *weakly coupled*. (Note that according to these definitions all concerted trajectories are strongly coupled.) Furthermore, we observed both adiabatic and nonadiabatic trajectories. Trajectories were labeled *adiabatic* if the system remained in the ground vibrational state throughout the trajectory and were labeled *nonadiabatic* if the system experienced nonadiabatic transitions among the vibrational states.

Table 1 lists the fraction of each type of trajectory that was observed in our ensemble of 89 trajectories. The trajectories were categorized by analyzing the expectation values of the two quantum proton coordinates as a function of time. (In this paper, all expectation values are calculated for the occupied adiabatic state.) We calculated the average time for double proton transfer (i.e., the time between the first proton breaking the bond with its donor and the second proton forming the bond with its acceptor) to be 0.4, 29.0, and 50.8 fs for concerted, strongly coupled sequential, and weakly coupled sequential trajectories, respectively. These numbers indicate that the entire process becomes faster as the coupling between the two reactions becomes stronger. Table 2 lists the various O−O distances for the model system at the beginning of the double proton transfer process (i.e., at the time the first proton breaks the bond with its donor) for strongly and weakly coupled trajectories. (As mentioned above, all concerted trajectories are considered strongly coupled, while sequential trajectories can be either

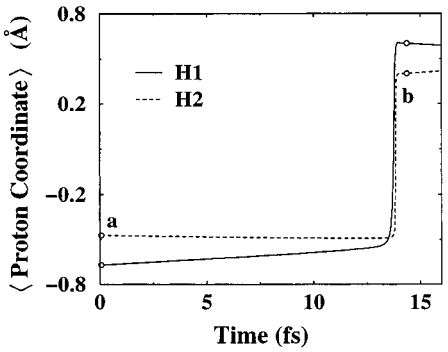

Figure 2. Time evolution of the expectation values of the coordinates of the quantum protons H1 and H2 (as labeled in Figure 1) for an adiabatic concerted trajectory. Each proton coordinate is measured relative to the midpoint between its donor and acceptor oxygen atoms. Expectation values are calculated for the occupied adiabatic state.

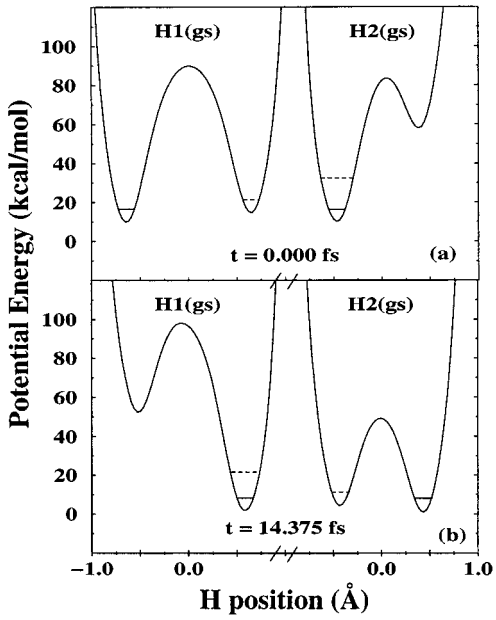

Figure 3. Effective potentials for protons H1 and H2 as a function of the proton coordinates at the times (a) and (b) labeled in Figure 2 for an adiabatic concerted trajectory. The ground vibrational state is indicated by a solid line, and the first excited vibrational state is indicated by a dashed line. For each proton, the occupied state is given in parentheses at the top, where (gs) denotes ground state and (es) denotes the first excited state.

strongly or weakly coupled.) Note that for all types of trajectories typically the first proton transfer reaction is initiated when the left and right solvating water molecules are approximately equal distances (∼2.8 Å) from the chain. Also note that the O−O distances are similar for strongly and weakly coupled trajectories, except for the distance between the H1 donor and acceptor; this distance is slightly longer for strongly coupled than for weakly coupled trajectories. This observation suggests that strong coupling between the two proton transfer reactions may result from destabilization of the extra proton on the middle water molecule of the chain caused by a longer O−O distance within the chain. We emphasize, however, that the statistical significance of these results is limited due to the small number of trajectories and that these results are not directly relevant to proton wires in proteins due to the simplicity of the model system.

One of the advantages of the MC-MDQT method is that it provides a clear physical framework for interpreting and analyzing the detailed proton transport dynamics. We have found

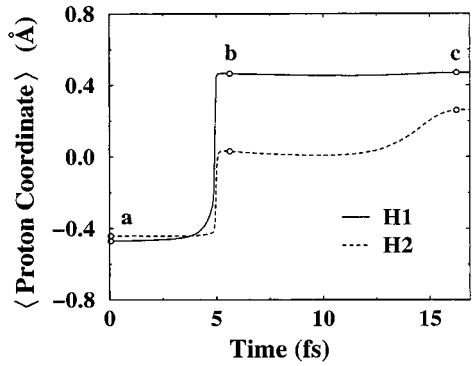

Figure 4. Time evolution of the expectation values of the coordinates of the quantum protons H1 and H2 for an adiabatic strongly coupled sequential trajectory.

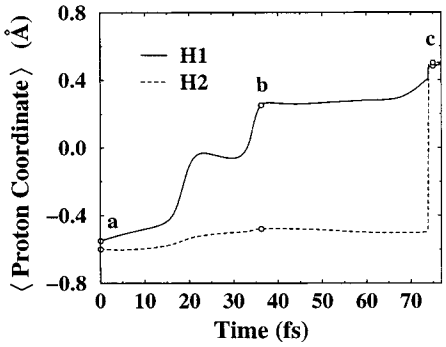

Figure 6. Time evolution of the expectation values of the coordinates of the quantum protons H1 and H2 for an adiabatic weakly coupled sequential trajectory. (This trajectory and the labeled times correspond to the snapshots depicted in Figure 1.)

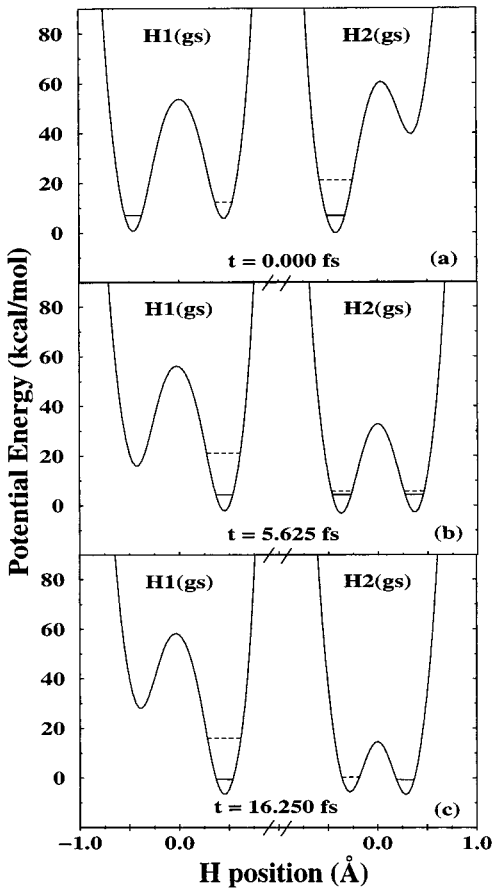

Figure 5. Effective potentials for protons H1 and H2 at the times (a), (b), and (c) labeled in Figure 4 for an adiabatic strongly coupled sequential trajectory.

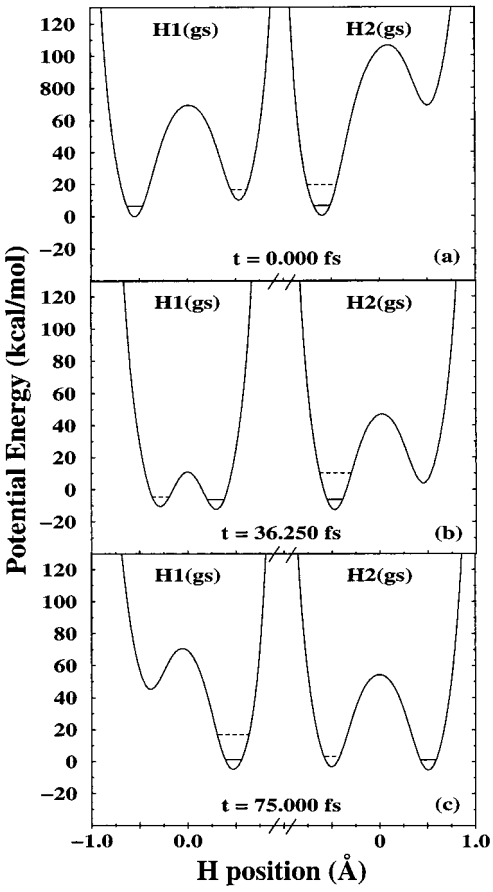

Figure 7. Effective potentials for protons H1 and H2 at the times (a), (b), and (c) labeled in Figure 6 for an adiabatic weakly coupled sequential trajectory.

that in proton transfer processes the wave functions are predominantly single configurational and multiconfigurational mixing is required only to convert from one single configurational wave function to another. As discussed in section II.A, a variational single configurational wave function can be calculated by the self-consistent solution of eqs 6 and 7 (with $Q = 1$). These equations indicate that, for single configurational wave functions, each proton can be viewed as occupying a single adiabatic state that can be calculated from a one-dimensional potential (which is derived from the classical configuration and the occupied adiabatic states of the other protons). Thus, we can elucidate the detailed motion of the individual protons and the correlation between them by plotting the effective potentials defined in eq 7 and calculating the corresponding adiabatic states by solving eq 6 for times along the trajectory when the wave function is primarily single configurational. The remainder of this section focuses on this type of analysis for five trajectories that represent the different types of processes observed.

First we analyze an adiabatic concerted trajectory. Figure 2 depicts the time evolution of the expectation values of the coordinates of the two quantum protons (labeled H1 and H2). Each quantum proton coordinate is measured relative to the midpoint between the donor and acceptor oxygen atoms, so a negative value indicates that the corresponding quantum proton is closer to its donor and a positive value indicates that the corresponding quantum proton is closer to its acceptor. Figure 2 indicates that for this trajectory both protons transfer at the same time. Figure 3 depicts the effective one-dimensional potentials for protons H1 and H2 at times $t = 0.000$ fs and $t =$

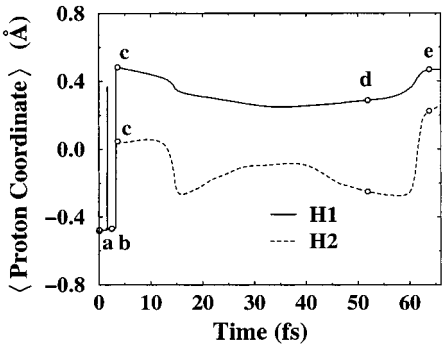

Figure 8. Time evolution of the expectation values of the coordinates of the quantum protons H1 and H2 for a nonadiabatic strongly coupled sequential trajectory.

14.375 fs, corresponding to the points labeled (a) and (b), respectively, in Figure 2. For each effective potential, the ground vibrational state is indicated by a solid line and the excited vibrational state is indicated by a dashed line. The label in parentheses at the top of each effective potential identifies the occupied one-particle adiabatic state for the corresponding quantum proton (where (gs) denotes ground state and (es) denotes the first excited state). Note that the barriers are relatively high for the trajectories presented in this paper due to the harmonic restraints on the oxygen atoms of the chain water molecules. At time (a) neither quantum proton has transferred, as indicated by the negative expectation values of the proton coordinates in Figure 2 and the localization of the occupied ground state in the reactant wells in Figure 3a. At time (b) both protons have transferred, as indicated by the positive expectation values of the proton coordinates and the localization of the occupied ground state in the product wells. Both quantum protons transferred due to ground state tunneling that occurred when both double wells were symmetrized simultaneously.

Figures 4 and 5 depict the analysis of an adiabatic strongly coupled sequential trajectory. At time (a) ($t = 0.000$ fs), neither proton has transferred. At time (b), ($t = 5.625$ fs) H1 has already transferred, as indicated by the positive expectation value for the H1 coordinate and the localization of the occupied ground state in the product well for H1. In contrast, at this same time (b) the double well potential for H2 is approximately symmetric and the occupied ground state is delocalized over both wells (which is also indicated by the expectation value of zero for the H2 coordinate). This symmetric configuration for H2 remains for almost 10 fs, until finally at time (c) ($t = 16.250$ fs) H2 is also transferred. Although both H1 and H2 transfer through ground state tunneling, the tunneling for H2 occurs over a much longer time scale than that for H1. Figure 5 also shows that both the distance between the minima and the barrier height decrease significantly for H2 throughout the trajectory, indicating that the donor and acceptor oxygen atoms for H2 move closer together (although the barrier is still substantially higher than the zero-point energy). This trajectory is labeled *sequential* because H1 is transferred by time (b), while H2 is not transferred until the later time (c). Moreover, this trajectory is labeled *strongly coupled* because when H1 is transferred at time (b) H2 is delocalized between its donor and acceptor.

Figures 6 and 7 depict the analysis of an adiabatic weakly coupled sequential trajectory. As in the previous cases, at time (a) ($t = 0.000$ fs) neither proton has transferred. At time (b) ($t = 36.250$ fs) H1 has transferred, as indicated by the positive expectation value of the H1 coordinate and the localization of the occupied ground state in the product well for H1. (Note that before transferring H1 spends more than 10 fs in a symmetric potential with the wave function delocalized over both wells, as indicated by the expectation value of zero for the H1 coordinate between (a) and (b).) In contrast, at time (b) H2 has not even started to transfer, as indicated by the negative expectation value of the H2 coordinate and the localization of the occupied ground state in the reactant well for H2. Although the energy of the product well for H2 has significantly decreased from time (a) to time (b), H2 does not transfer until more than 30 fs later at time (c) ($t = 75.000$ fs). Again both H1 and H2 transfer through ground-state tunneling, although in this case the tunneling for H1 occurs on a longer time scale than that for

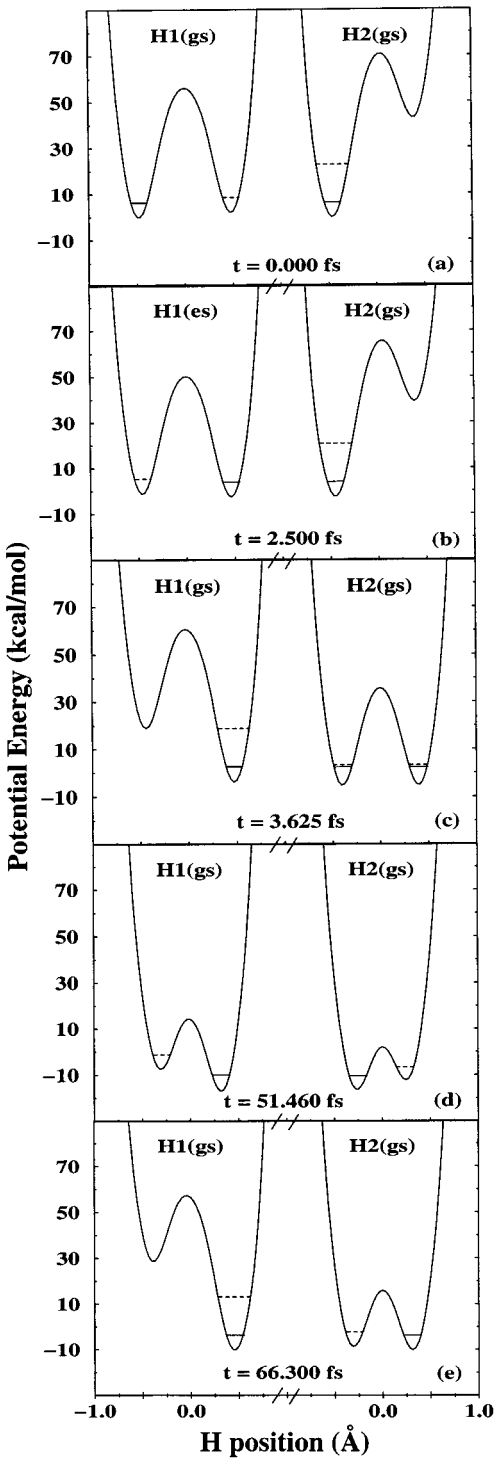

Figure 9. Effective potentials for protons H1 and H2 at the times (a), (b), (c), (d), and (e) labeled in Figure 8 for a nonadiabatic strongly coupled sequential trajectory.

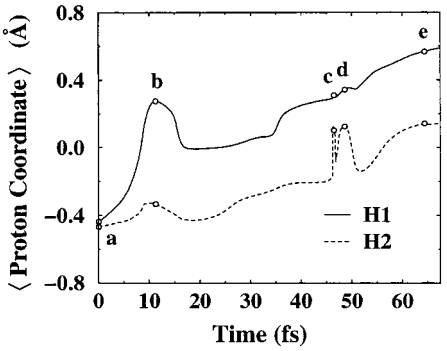

Figure 10. Time evolution of the expectation values of the coordinates of the quantum protons H1 and H2 for a nonadiabatic weakly coupled sequential trajectory.

H2. This trajectory is labeled *sequential* because H1 is transferred at time (b) while H2 is transferred more than 30 fs later at time (c), and this trajectory is labeled *weakly coupled* because the two protons move almost independently.

Figures 8 and 9 depict the analysis of a nonadiabatic strongly coupled sequential proton transfer. At time (a) ($t = 0.000$ fs) both protons are in the ground state and are localized in the reactant wells. At time (b) ($t = 2.500$ fs) H1 occupies the excited state, which is localized in the reactant well. The spike between (a) and (b) in Figure 8 indicates that H1 is instantaneously localized near the product well immediately prior to the nonadiabatic transition, which occurs when the double well potential for H1 is nearly symmetric. (Note that the first proton is not considered to be transferred at this spike because the OH bond is not fully formed.) By time (c) ($t = 3.625$ fs), H1 has switched back down to the ground state and is fully transferred. At this same time (c), the double well potential for H2 has become approximately symmetric, so the occupied ground state is delocalized over both wells and the expectation value for the H2 coordinate is zero. At time (d) ($t = 51.460$ fs), H2 is localized on the reactant side again, and by time (e) ($t = 66.300$ fs) H2 is finally transferred. This trajectory is labeled *sequential* since H1 is transferred by time (c) while H2 is not transferred until time (e). Moreover, this trajectory is labeled *strongly coupled* because when H1 is transferred at time (c) H2 is delocalized between its donor and acceptor.

Figures 10 and 11 depict the analysis of a nonadiabatic weakly coupled sequential trajectory. At time (a) ($t = 0.000$ fs) both protons are in the ground state and are localized in the reactant wells. At time (b) ($t = 11.250$ fs) H1 has transferred, as indicated by the positive expectation value for the H1 coordinate and the localization of the occupied ground state in the product well for H1. At this time (b) H2 has not yet transferred and is still localized in the reactant well. In the time between (b) and (c), the wave function for H1 becomes delocalized again (as indicated by the expectation value for the H1 coordinate returning to zero for approximately 20 fs). At time (c) ($t = 46.500$ fs) H1 is transferred again. Also at time (c) the double well potential for H2 is symmetrized so the wave function is delocalized over both wells, and H2 occupies the excited state (i.e., H2 has experienced a nonadiabatic transition). At time (d) ($t = 48.625$ fs) H2 is still in this symmetrized configuration but occupies the ground state, and by time (e) ($t = 64.375$ fs) H2 has transferred. Note that both the distance between the minima and the barrier height decrease significantly for H2 throughout the trajectory, indicating that the donor and acceptor oxygen atoms for H2 move much closer together. This trajectory is labeled *sequential* because H1 is first transferred at time (b) while H2 is not transferred until time (e). Moreover, this

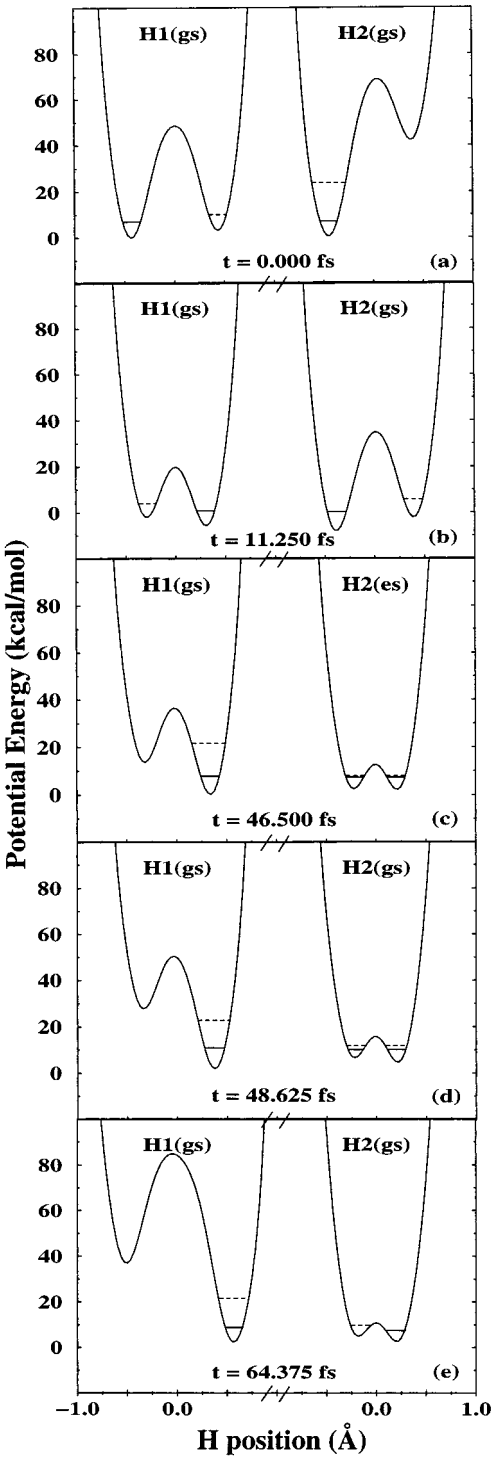

Figure 11. Effective potentials for protons H1 and H2 at the times (a), (b), (c), (d), and (e) labeled in Figure 10 for a nonadiabatic weakly coupled sequential trajectory.

trajectory is labeled *weakly coupled* because when H1 is first transferred at time (b) H2 has not even started to transfer. (We emphasize, however, that this labeling is somewhat misleading for this trajectory since after time (b) H1 becomes delocalized and transfers again at time (d) with strong coupling to H2.)

IV. Conclusions

We have utilized the MC-MDQT method to perform non-equilibrium real-time quantum dynamical simulations of proton transport along water chains in the presence of solvating water

molecules. Our model system consists of a protonated chain of three water molecules with two solvating water molecules hydrogen-bonded to each end of the chain. Our simulations indicate that solvation and hydrogen bonding significantly impact the proton transport process and that quantum effects such as hydrogen tunneling and nonadiabatic transitions play an important role. Moreover, we found that this model system exhibits a wide range of mechanisms, including both concerted and sequential double proton transfer, both strongly and weakly coupled double proton transfer, and both adiabatic and nonadiabatic pathways. The MC-MDQT approach provides a clear physical framework for interpreting and analyzing these different types of mechanisms. We found that the proton vibrational wave functions are predominantly single configurational and that multiconfigurational mixing is required only to switch from one single configuration to another. For single configurational wave functions, each proton can be viewed as occupying a single adiabatic state that can be calculated from an effective one-dimensional potential (which is derived from the classical configuration and the occupied adiabatic state). These effective one-dimensional potentials and the corresponding one-particle adiabatic states can be calculated along a trajectory to elucidate both the detailed quantum dynamical motion of the individual protons and the correlation among the multiple proton transfer reactions.

The motivation for these simulations was to enhance our understanding of solvation and hydrogen-bonding effects for the process of proton transport along water chains in proteins. Clearly the model systems studied in this paper do not adequately represent water chains in protein environments. Nevertheless, these model systems have allowed us to investigate a number of possible dynamical mechanisms and to develop an analysis scheme that will be useful for future studies in more realistic protein environments.

Acknowledgment. We gratefully acknowledge financial support from the NSF CAREER program Grant CHE-9623813, the Petroleum Research Fund (administered by the ACS) Grant 30432-G6, and the Clare Boothe Luce Foundation. H.D. acknowledges the University of Minnesota-IBM Shared Research Project and the National Science Foundation (Grant CDA-9502979). S.H.-S. is a recipient of an Alfred P. Sloan Research Fellowship.

References and Notes

(1) Baciou, L.; Michel, H. *Biochemistry* **1995**, *34*, 7967.
(2) Martinez, S. E.; Huang, D.; Ponomarev, M.; Cramer, W. A.; Smith, J. L. *Protein Sci.* **1996**, *5*, 1081.
(3) von Grotthus, C. J. D. *Ann. Chim. LVIII* **1806**, 54.
(4) Pomès, R.; Roux, B. *Chem. Phys. Lett.* **1995**, *234*, 416.
(5) Pomès, R.; Roux, B. *J. Phys. Chem.* **1996**, *100*, 2519.
(6) Pomès, R.; Roux, B. *Biophys. J.* **1998**, *75*, 33.
(7) Lobaugh, J.; Voth, G. A. *J. Chem. Phys.* **1996**, *104*, 2056.
(8) Schmitt, U.; Voth, G. A. *J. Phys. Chem. B* **1998**, *102*, 5547.
(9) Duan, X.; Scheiner, S. *J. Mol. Struct.* **1992**, *270*, 173.
(10) Cheng, H.-P.; Barnett, R. N.; Landman, U. *Chem. Phys. Lett.* **1995**, *237*, 161.
(11) Laasonen, K.; Sprik, M.; Parrinello, M.; Car, R. *J. Chem. Phys.* **1993**, *99*, 9080.
(12) Tuckerman, M.; Laasonen, K.; Sprik, M.; Parrinello, M. *J. Chem. Phys.* **1995**, *103*, 150.
(13) Tuckerman, M. E.; Marx, D.; Klein, M. L.; Parrinello, M. *Science* **1997**, *275*, 817.
(14) Sagnella, D. E.; Laasonen, K.; Klein, M. L. *Biophys. J.* **1996**, *71*, 1172.
(15) Kreuer, K.-D. *Chem. Mater.* **1996**, *8*, 610.
(16) Schmidt, R. G.; Brickmann, J. *Ber. Bunsen-Ges. Phys. Chem.* **1997**, *101*, 1816.
(17) Agmon, N. *Chem. Phys. Lett.* **1995**, *244*, 456.
(18) Billeter, S. R.; van Gunsteren, W. F. *Comput. Phys. Comm.* **1997**, *107*, 61.
(19) Vuilleumier, R.; Borgis, D. *Chem. Phys. Lett.* **1998**, *284*, 71.
(20) Vuilleumier, R.; Borgis, D. *J. Phys. Chem. B* **1998**, *102*, 4261.
(21) Hammes-Schiffer, S. *J. Chem. Phys.* **1996**, *105*, 2236.
(22) Drukker, K.; Hammes-Schiffer, S. *J. Chem. Phys.* **1997**, *107*, 363.
(23) Drukker, K.; de Leeuw, S.; Hammes-Schiffer, S. *J. Chem. Phys.* **1998**, *108*, 6799.
(24) Meyer, E. *Protein Sci.* **1992**, *1*, 1543.
(25) Pomès, R.; Roux, B. *Biophys. J.* **1996**, *71*, 19.
(26) Morillo, M.; Cukier, R. I. *J. Chem. Phys.* **1990**, *92*, 4833.
(27) Suárez, A.; Silbey, R. *J. Chem. Phys.* **1991**, *94*, 4809.
(28) Warshel, A.; Chu, Z. T. *J. Chem. Phys.* **1990**, *93*, 4003.
(29) Aqvist, J.; Warshel, A. *Chem. Rev.* **1993**, *93*, 2523.
(30) Truhlar, D. G.; Liu, Y.-P.; Schenter, G. K.; Garrett, B. C. *J. Phys. Chem.* **1994**, *98*, 8396.
(31) Borgis, D.; Tarjus, G.; Azzouz, H. *J. Phys. Chem.* **1992**, *96*, 3188.
(32) Borgis, D.; Tarjus, G.; Azzouz, H. *J. Chem. Phys.* **1992**, *97*, 1390.
(33) Laria, D.; Ciccotti, G.; Ferrario, M.; Kapral, R. *J. Chem. Phys.* **1992**, *97*, 378.
(34) Borgis, D.; Hynes, J. T. *Chem. Phys.* **1993**, *170*, 315.
(35) Mavri, J.; Berendsen, H. J. C.; van Gunsteren, W. F. *J. Phys. Chem.* **1993**, *97*, 13469.
(36) Mavri, J.; Berendsen, H. J. C. *J. Phys. Chem.* **1995**, *99*, 12711.
(37) Staib, A.; Borgis, D.; Hynes, J. T. *J. Chem. Phys.* **1995**, *102*, 2487.
(38) Ando, K.; Hynes, J. T. *J. Mol. Liq.* **1995**, *64*, 25.
(39) Bala, P.; Lesyng, B.; McCammon, J. A. *Chem. Phys.* **1994**, *180*, 271.
(40) Bala, P.; Grochowski, P.; Lesyng, B.; McCammon, J. A. *J. Phys. Chem.* **1996**, *100*, 2535.
(41) Hammes-Schiffer, S.; Tully, J. C. *J. Chem. Phys.* **1994**, *101*, 4657.
(42) Hammes-Schiffer, S.; Tully, J. C. *J. Phys. Chem.* **1995**, *99*, 5793.
(43) Li, D.; Voth, G. A. *J. Phys. Chem.* **1991**, *95*, 10425.
(44) Hwang, J.-K.; Warshel, A. *J. Phys. Chem.* **1993**, *97*, 10053.
(45) Hwang, J.-K.; Chu, Z. T.; Yadav, A.; Warshel, A. *J. Phys. Chem.* **1991**, *95*, 8445.
(46) Lobaugh, J.; Voth, G. A. *Chem. Phys. Lett.* **1992**, *198*, 311.
(47) Lobaugh, J.; Voth, G. A. *J. Chem. Phys.* **1994**, *100*, 3039.
(48) Azzouz, H.; Borgis, D. *J. Chem. Phys.* **1993**, *98*, 7361.
(49) Hammes-Schiffer, S. *Advances in Classical Trajectory Methods*; JAI Press Inc.: London, 1998; Vol. 3, pp 73−119.
(50) Hammes-Schiffer, S. *J. Phys. Chem. A* **1998**, *102*, 10443.
(51) Tully, J. C. *J. Chem. Phys.* **1990**, *93*, 1061.
(52) We observed a large number of classically forbidden transitions in the simulations presented in this paper. Recently, our group devised a modification of MDQT that eliminates these classically forbidden transitions and thus ensures consistency between the quantum probabilities and the fraction of trajectories in each state.[53] This new method will be incorporated into future simulations.
(53) Fang, J.-Y.; Hammes-Schiffer, S. *J. Chem. Phys.* (in press).
(54) Morelli, J.; Hammes-Schiffer, S. *Chem. Phys. Lett.* **1997**, *269*, 161.
(55) Fang, J.-Y.; Hammes-Schiffer, S. *J. Chem. Phys.* **1997**, *107*, 8933.
(56) Stillinger, F. H.; David, C. W. *J. Chem. Phys.* **1978**, *69*, 1473.
(57) Weber, T. A.; Stillinger, F. H. *J. Phys. Chem.* **1982**, *86*, 1314.
(58) Stillinger, F. H. *J. Chem. Phys.* **1979**, *71*, 1647.
(59) Andersen, H. C. *J. Comput. Phys.* **1983**, *52*, 24.
(60) Nosé, S. *J. Chem. Phys.* **1984**, *81*, 511.
(61) Hoover, W. G. *Phys. Rev. A* **1984**, *31*, 1695.